Journal of Instrumentation

Characterization and core renovation of beam stoppers for personnel safety

Published by IOP Publishing for Sissa Medialab

Received: *October 21, 2018*
Accepted: *January 11, 2019*
Published: *January 30, 2019*

TECHNICAL REPORT

Characterization and core renovation of beam stoppers for personnel safety

A. Pilan Zanoni,[1] J.A. Briz Monago, E. Grenier-Boley, M. Calviani and V. Vlachoudis

CERN, CH-1211 Geneva, Switzerland

E-mail: andre.pilan.zanoni@cern.ch

Abstract: To minimize the risk of accident on personnel accessing the PS complex at CERN transfer lines are equipped with beam stoppers. They immediately shut the beam aperture whenever members of personnel enter an accelerator or test facility. Most of them consist of cores out of stainless steel designed for a proton beam-pulse energy at 9.0 kJ during the 70's. Further data on the design history of the beam stoppers is scarce. With the current pulse energy at 35.0 kJ steel reaches its structural limits. Based on the current function of the core requirements on the structural and beam-interaction performance of beam stoppers for personnel safety are drawn. To meet those requirements a compact core compatible to all PS complex is developed, replacing five existing design types. The new core introduces high-density sliced materials which withstand upgraded beam-pulse energies up to 92.5 kJ.

Keywords: Accelerator Subsystems and Technologies; Instrumentation for particle accelerators and storage rings - high energy (linear accelerators, synchrotrons); Overall mechanics design (support structures and materials, vibration analysis etc)

[1]Corresponding author.

https://doi.org/10.1088/1748-0221/14/01/T01011

2019 JINST 14 T01011

Contents

2019 JINST 14 T01011

1 Introduction

Particles sent to the Large Hadron Collider (LHC) at CERN are first accelerated in the Proton Synchrotron (PS). It is fed by the Proton Synchrotron Booster (PSB) with four stacked synchrotron rings that receive protons from linear accelerators. Not only does PS extract LHC-dedicated beam, but it also provides the neutron Time-of-Flight facility (nTOF) [1], the Antiproton Decelerator (AD) [2] and the East Area (EA) [3] with protons up to 26 GeV/c.

The risk of beam accident of technical personnel intervening in the different facilities and acceleration stages has to be the lowest. In order to mitigate this probability Elements Important for Safety type beam (EIS-b) are installed in the beam transfer lines [4, 5]. For redundancy each transfer line has two independent EIS-b of two different operating modes: a magnetic bender and a beam-intercepting material block [6]. In normal beam operation both EIS-b do not interact with the

beam, however they are actuated during intervention campaigns or personnel intrusion to a facility. Secondary particles produced by the beam impact in the block are absorbed by external shielding.

A beam stopper consists of that block, which is also referred to as core, in a vacuum chamber. The design criterion met in the 70's was to use common, reliable and cheap materials which could sustain one beam impact of 2×10^{12} particles per pulse at 28 GeV [7]. Stainless steel was chosen as the core material because the beam power was considered negligible [7]. Since then no further design record has been available and the thermal and structural performance of the PS beam stoppers are yet to be analyzed. Documentation on the minimum core size, structural criterion for the core, actuation time and maximum number of allowed pulses is scarce or non-existent.

The highest beam intensity has been increased to 8.7×10^{12} ppp (particles per pulse) at 26 GeV/c for nominal LHC beam and to 20×10^{12} ppp at 14 GeV/c for machine development campaigns [8]. In the framework of the LHC Injectors Upgrade (LIU) [9, 10] those intensities may be further increased to 23×10^{12} and 50×10^{12} ppp respectively [8].

The goal of this paper is to first analyze the thermo-mechanical and beam-attenuation performance of the beam stoppers currently active in the PS complex. Using their configuration and best practices we specify guidelines for a beam stopper design and devise beam stopper cores capable of receiving high-intensity beams.

2 Current beam stoppers

In this section we present the operation and describe the different design types of the beam stoppers existent in the PS complex.

2.1 Operation

The position of the stopper core is managed by the personnel access system [6, 11] which is dedicated to personnel access to beam facilities and independent from the control system of the accelerator machine [11].

During beam operation the stopper core rests out of the beam line (OUT-BEAM position). The core is linked to a one-way pneumatic actuator at 4 bar while the solenoid of the pneumatic valve is powered at 25 V (figure 1a). The air pressure force balances the weight of the core. By cutting the power supply in the solenoid the air pressure in the pneumatic actuator is released, inverting the resultant force in the actuator. The core is left to fall in beam line (IN-BEAM position), until reaching an end stop (figure 1b). The IN-BEAM and OUT-BEAM positions are read by end-switches. Any intermediate position is not detected [12].

The actuation of the beam stopper is fail-safe because its core moves always in beam position whenever power cut or air-pressure failure in the stopper occur. The core also moves in beam position when [6]:

- a beam operator grants access to the downstream facility. The beam is already dumped upstream and does not hit the stopper core.
- someone forces an access door of a downstream accelerator. The access system automatically moves the upstream stopper core in beam position before the beam is dumped. This is an accidental case as the beam hits the material core.

2019 JINST 14 T01011

Upon permission of the downstream areas [6] the personnel access system puts the beam stopper out of the beam line by energizing the solenoid and pressurizing the cylinder.

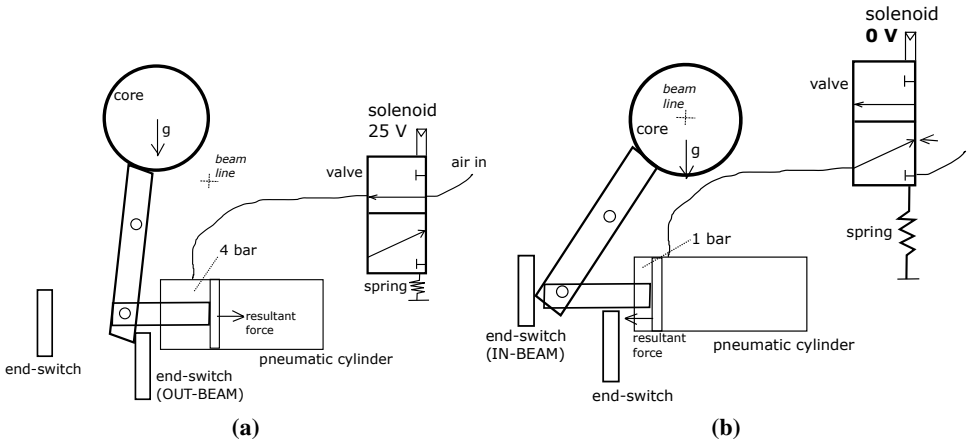

Figure 1. Schematic representation of the single-way actuation of the beam stopper core with pivot mechanism. (a) OUT-BEAM position. (b) IN-BEAM position.

2.2 Beam-stopper types

The PS complex (figure 2) has six types of beam stoppers (figure 3).

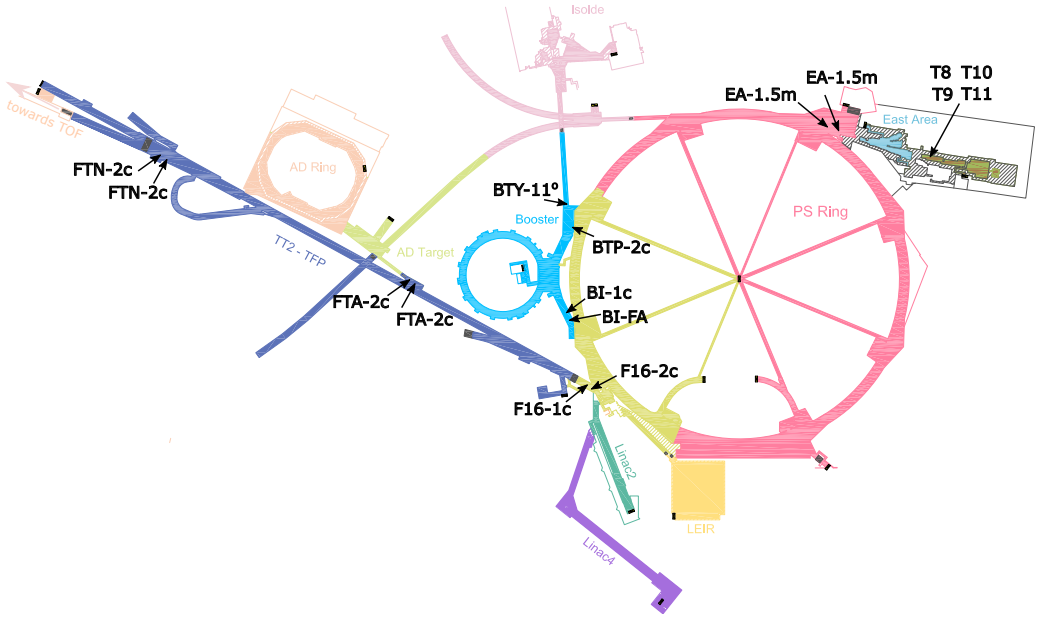

Figure 2. Map of the beam stoppers in the PS complex today.

The BI-FA stopper lies in the PSB injection line (BI) and has a pivot mechanism. The stopper core has four concentric 170-mm-long cylindrical shells out of graphite wedged in a round plate. Dimension of the shells (diameter × thickness): ⌀120 mm × 1.6 mm, ⌀130 mm × 1.75 mm, ⌀140 mm × 1.85 mm and ⌀150 mm × 2.1 mm. The core travels 150 mm in 3 seconds. The beam

2019 JINST 14 T01011

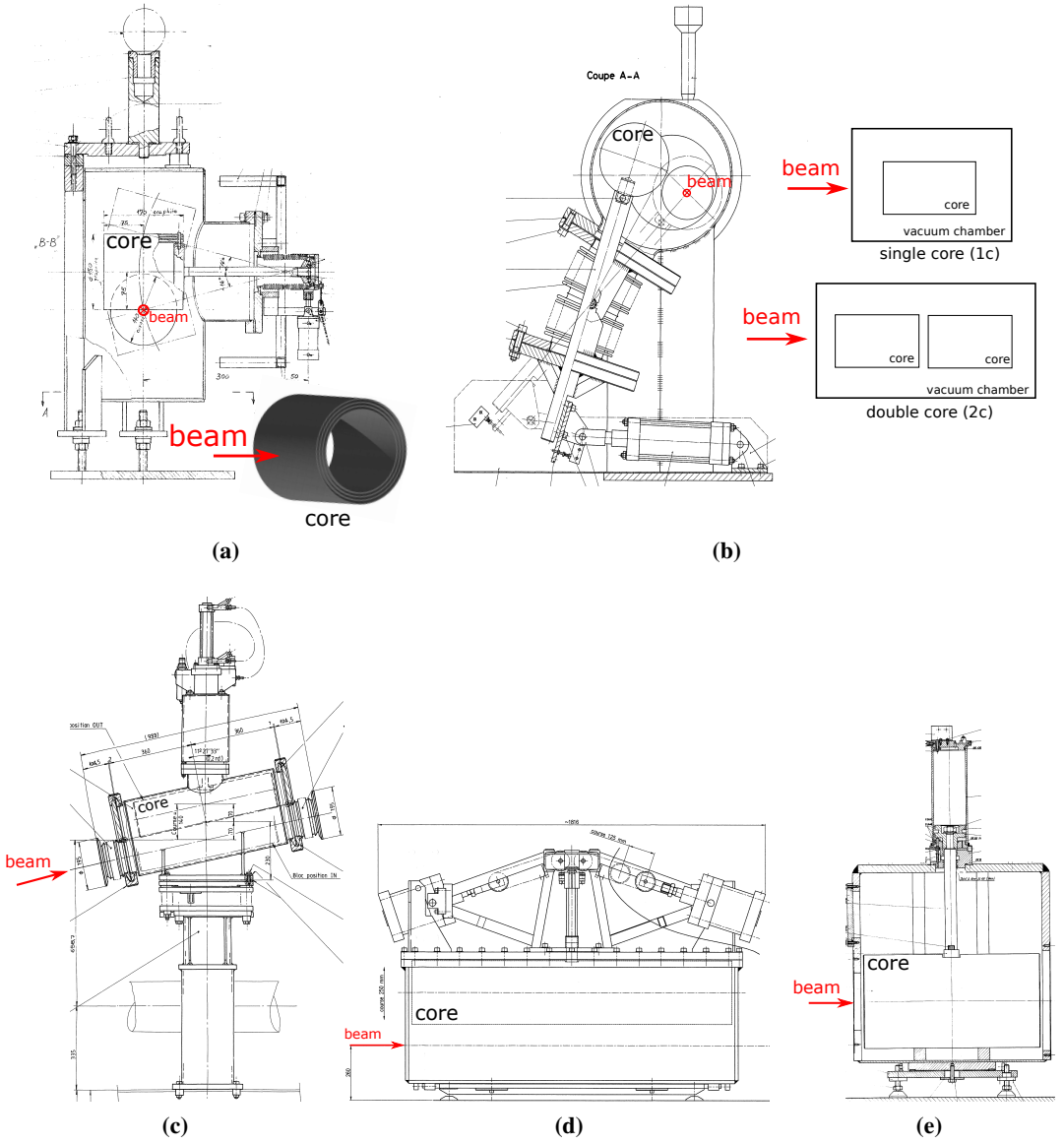

Figure 3. Design types of the beam stoppers in the PS complex today. (a) BI-FA, (b) 1c/2c, (c) BTY-11°, (d) EA-1.5m, (e) EA-TX.

hits the shells radially interacting with a total of 14.6-mm material depth. Except for BI-FA all PS stopper cores are massive cylinders out of steel for axial beam impacts.

Downstream in the BI line a stopper type 1c out of stainless steel provides a core length of 600 mm. The core is pivoted and has a diameter of ⌀200 mm.

In the transfer lines in the PS injection (BTP), extraction (F16), AD (FTA) and nTOF (FTN) a combination of stoppers type 1c and 2c are used to increase the total length for beam attenuation. The stopper type 2c has two mechanically independent cores in the same vacuum chamber. However their control systems are linked and both cores can only be moved simultaneously in beam line.

2019 JINST 14 T01011

Each core has a diameter of ⌀200 mm and a length of 550 mm spaced by 50 mm. Both 1c and 2c cores travel 175 mm in less than 17 seconds.

The beam stopper in the transfer line to ISOLDE (BTY-11°) has a core tilt of 11° and a vertical pneumatic mechanism. The core is made of stainless steel 304 and has a diameter of ⌀140 mm with a length of 600 mm. The beam aperture of 140 mm is closed in 4 seconds.

The extraction line to the East Area has two beam stoppers type EA-1.5m. Each core is made of CK45 steel with 1.5-m length and a diameter of ⌀300 mm. It is screwed to a driving mechanism consisting of forks and chains. The core falls 260 mm in 17 seconds.

Each experimental line inside the East area — T8, T9, T10, T11 — is equipped with a beam stopper type EA-TX. The core is made of iron coated with copper and has a diameter of ⌀300 mm and a length of 600 mm. The core falls 260 mm in less than 30 seconds actuated by a vertical pneumatic cylinder.

3 Methods and core requirements

In accidental scenarios beam hits the stopper core. The core must be able to attenuate a great amount of beam particles while resisting high thermal stresses caused by accidental impacts of particle beam pulses. In this section we introduce methods for modeling the thermo-mechanical and beam-attenuation performance of the current stopper cores.

3.1 Thermo-mechanical modeling

The interaction between beam and matter induces focused heat deposition in the core material. We use the Monte Carlo particle transport and interaction code FLUKA [13, 14] to simulate the energy deposited in the core material normalized to one particle. The energy density per beam particle (Q_{bp}) is converted to power density per pulse ($\dot{Q}_{\mathrm{pulse}}$) through eq. 3.1.

$$\dot{Q}_{\mathrm{pulse}} = \frac{Q_{\mathrm{bp}} n_{\mathrm{p}}}{\mu} \tag{3.1}$$

Here n_{p} is the number of particles per pulse and μ the beam pulse length. For bunched beams μ corresponds to the number of bunches multiplied by the bunch length.

The energy deposited in the stopper core is imported as internal heat generation in a thermal model in ANSYS 17.1. In our models we calculate the difference in the imported energy between ANSYS 17.1 and FLUKA to be less than 0.1%. The difference in the peak temperature in both models is smaller than 1.2%. The thermal model in ANSYS 17.1 determines the temperature distribution through eq. 3.2 [15].

$$\rho(T) c_{\mathrm{p}}(T) \left(\frac{\partial T}{\partial t} \right) + \nabla(k(T)T) = \dot{Q}_{\mathrm{pulse}} \tag{3.2}$$

Where T is the temperature, t the time, ρ the mass density, c_{p} the specific heat capacity and k the thermal conductivity.

The temperature distribution at each time step is imported in an ANSYS 17.1 structural model [15] which is solved through implicit methods such as [16] and [17]. Our maximum time step length (Δt) for structural simulations follows the Courant-Friedrichs-Lewy condition (eq. 3.3) [18].

2019 JINST 14 T01011

Here c is the speed of sound in the material (eq. 3.4), E the Young's modulus and ν the Poisson's ratio.

$$\Delta t < \frac{l}{c} \tag{3.3}$$

$$c = \sqrt{\frac{E}{\rho(1-\nu^2)}} \tag{3.4}$$

The initial temperature for all simulations is 22°C. Because of vacuum there is no convective heat exchange in the core. For stainless steel the emissivity factor for the radiative transfer between the core and the vacuum chamber is assumed to be 0.5. In the structural model the core is fixed through weak springs [15].

For the thin graphite BI-FA core the thermo-mechanical performance is computed via layered shell elements [19]. To quickly assess the material integrity we use the Coulomb-Mohr criterion [20]. Here a safety factor $F < 1$ indicates the material is safe.

The metallic cores are modeled with solid elements and evaluated through the von-Mises yield criterion [21, 22]. Considering σ_e the equivalent von-Mises stress and $\sigma_y(T)$ the temperature-dependent tensile yield strength a value $\sigma_e/\sigma_y(T) < 1$ indicates the deformation induced by thermal gradients is reversible (elastic), otherwise it is permanent (plastic).

3.2 Beam attenuation

At low energies a particle beam is stopped mainly due to ionization losses in the intercepting material. Due to the increasing cross section interaction and the decreasing particle's energy through matter the primary particles come to a complete stop at a characteristic material depth — the projected range [23].

At high beam energies inelastic nuclear scattering [24] with target nuclei becomes more relevant than ionization losses. The inelastic nuclear scattering length λ_{inel} (eq. 3.5 [25]) describes the length of target material in which the intensity of the beam is reduced to 1/e (≈ 0.368) of the initial intensity due to inelastic nuclear scattering interactions in the target. It quantifies the beam attenuation produced via inelastic nuclear scattering.

$$\frac{I}{I_0} = e^{-\frac{L}{\lambda_{\text{inel}}}} \tag{3.5}$$

Here I_0 is the initial intensity of a particle beam impinging on the target, I the beam intensity that passes through the target without undergoing inelastic nuclear scattering, λ_{inel} the inelastic nuclear scattering length and L the length of a target. Table 1 shows the values of λ_{inel} for materials used in today's stoppers.

Ionization losses are dominant for proton energies lower than 160 MeV incident on today's core materials. There the projected range is shorter than the nuclear interaction length. On the contrary, at beam energies higher than 1.4 GeV, nuclear interaction becomes dominant. The length of the stopper core depends on the projected range at low beam energies and the nuclear interaction length at high beam energies.

We assess the lateral containment of electromagnetic shower of particles produced by the beam-matter interaction via the Molière radius R_m [26]. A cylinder with the radius of 3.5 R_m is

2019 JINST 14 T01011

Table 1. Projected range due to ionization losses and inelastic nuclear scattering length λ_{inel} of the different materials and proton energies currently used in the PS complex at CERN calculated with FLUKA [13, 14].

material	proton energy [GeV]	projected range [mm]	λ_{inel} [mm]
graphite	0.05	11	331
graphite	0.16	87	485
steel	0.05	4.2	122
steel	0.16	32	177
steel	1.4	998	153
steel	2	1430	150
steel/iron	25.1	> 8000	156

able to absorb 99% of the energy of the electromagnetic shower produced after the interaction of the beam with the target [27]. For steel R_{m} = 17.6 mm [28]. Most of the stopper cores in the PS complex are made of steel and have a radius of 100 mm which corresponds to 5.7 R_{m}.

4 Results of current stopper cores

This section discusses the performance of the current beam stoppers on the perspective of thermal and structural response. The beam parameters for the analysis are summarized in table 2, where σ_{x} and σ_{y} are the beam sizes at 1 σ following a two-dimensional Gaussian profile.

Table 2. Proton beam parameters at the positions of beam stoppers in the PS complex. * denotes upgraded beam parameters.

Beam stopper	σ_{x/σ_y} [mm]	number of bunches per pulse	particles per pulse $\times 10^{12}$	bunch length	beam energy
BI-FA [29]	4.41/3.18	-	127	120 μs	50 MeV
BI-FA* [29]	2.35/3.01	-	100	400 μs	160 MeV
BI-SW [29]	6.32/6.50	-	127	120 μs	50 MeV
BI-SW* [29]	3.08/2.86	-	100	400 μs	160 MeV
BTP [30]	2.90/2.90	4	13	201 ns	2.0 GeV
BTY [31]	3.80/2.70	4	40	230 ns	1.4 GeV
BTY* [31]	3.90/2.50	4	64	230 ns	2.0 GeV
EA* [32]	5.0/5.0	-	0.5	0.4 s	24 GeV/c
F16 [8]	1.15/1.05	8	5.8	180 ns	26 GeV/c
F16* [8]	1.50/1.39	6	23	180 ns	26 GeV/c
FTA [8]	4.57/5.25	4	17	185 ns	26 GeV/c
FTN [8]	9.04/3.00	1	8.5	190 ns	20 GeV/c

4.1 BI line

For the BI-FA stopper core the two inner shells are modeled with two layers, the two outer shells with 30 layers using layered shell elements [19].

2019 JINST 14 T01011

Figure 4 shows the Bragg peak, the point at maximum beam energy deposition due to ionization, lies between the last shells hit by a 50-MeV proton beam. We calculate more than 99% of the energy of the incoming primary particles is absorbed by this core, while the energy absorbed by BI-SW is nearly zero. The material is safe as the maximum $F = 0.19$ in the core material.

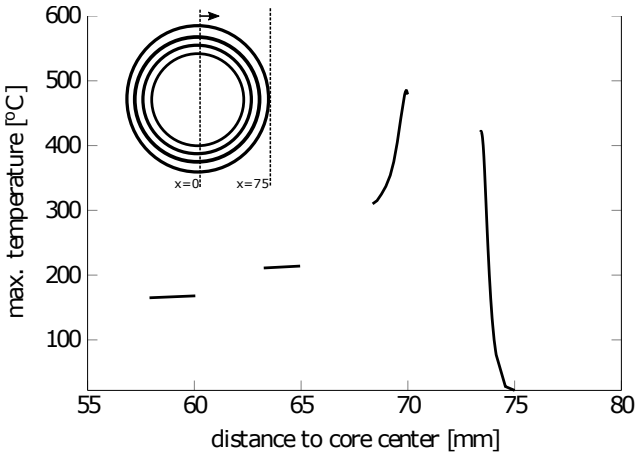

Figure 4. Through-thickness temperature distribution in the beam axis in the core layers from a 50-MeV proton beam.

Increasing the proton energy to 160 MeV causes most of the beam particles to pass through the graphite core. Only 10.3% of the incoming beam energy is absorbed by the BI-FA and 94% by the BI-SW core. The peak temperature in all shells is nearly the same at 199°C with a maximum safety factor $F = 0.12$. Due to the beam dilution caused by BI-FA the peak temperature rise per pulse is only 7.2°C in the BI-SW core.

In case the actuation of the BI-FA core fails a single beam impact causes concentrated plastic deformation in the BI-SW core due to short beam projected ranges. The peak equivalent stress is evaluated at 210 MPa for the 50-MeV beam and 397 MPa for the 160-MeV beam, exceeding the elastic limit of stainless steel [33]. In addition the BI-SW core is exposed to excessive peak temperature rise of $T_{\max} = 385$°C (50 MeV) and 750°C (160 MeV).

During the next long shutdown at CERN both BI-FA and BI-SW stoppers will be dismantled. The personnel protection system of the BI line will be integrated to Linac4 [34] where a beam stopper core out of a graphite R4550 rod (⌀80 mm x 120 mm) shrink-fit in a stainless steel clad withstands few 160-MeV proton beam pulses [35].

4.2 Current stoppers with steel cores

We evaluate the ratio between the equivalent stress and the temperature-dependent yield strength in the geometric model of the steel cores (table 3). For the core material to be safe max $\sigma_e/\sigma_y(T) < 1$.

For 20 repeated pulses on the BTP stopper $T_{\max} = 90.1$°C and $\sigma_e/\sigma_y(T) = 0.64$. In case a BTY beam hits the BTP stopper, e.g. due to a failure on the beam transfer, the BTP core presents some plastic deformation after three repeated pulses.

A cycle of six spills can hit the EA stopper core after the slow beam extraction from the Proton Synchroton to the East area [32]. Each spill is 0.4-second long repeating each 2.4 seconds. The

2019 JINST 14 T01011

Table 3. Peak temperature, maximum $\sigma_e/\sigma_y(T)$ from one proton beam pulse and minimum number of repeated pulses to plastic deformation in steel cores. Repetition rate: 1.2 s

Beam scenario	peak temperature [°C]	maximum $\sigma_e/\sigma_y(T)$ one pulse	repeated pulses for $\sigma_e/\sigma_y(T) > 1$
BTP*	39.9	0.25	indefinite
BTY	66.7	0.58	3
BTY*	100.6	1.02	1
EA*	24.0	0.01	indefinite
F16	114.6	1.06	1
F16*	250.4	1.14	1
FTA	51.7	0.56	2
FTN	33.6	0.27	5

cycles are spaced by 45.6 seconds. After each cycle $T_{max} = 25.7$°C, maximum $\sigma_e/\sigma_y(T) = 0.04$ and maximum $\sigma_e = 6.7$ MPa.

Critical beam scenarios are those of F16 and the upgraded BTY in which one single pulse causes plastic deformation. Although the stopper core is still operational the accumulation of plastic deformation under frequently repeated pulses lead to the start of fracturing (figure 5a). Once the yield strength is reached adding more thermal strain increases the plastic strain ε_p, conducting to the start of fracture at $\varepsilon_{tensile}$. For stainless steel $\varepsilon_{tensile}$ is about 0.2 [36]. Leaving the stopper core to be cooled down over long periods between beam impacts dampens the increase of plastic strain in the F16 stopper core (figure 5b).

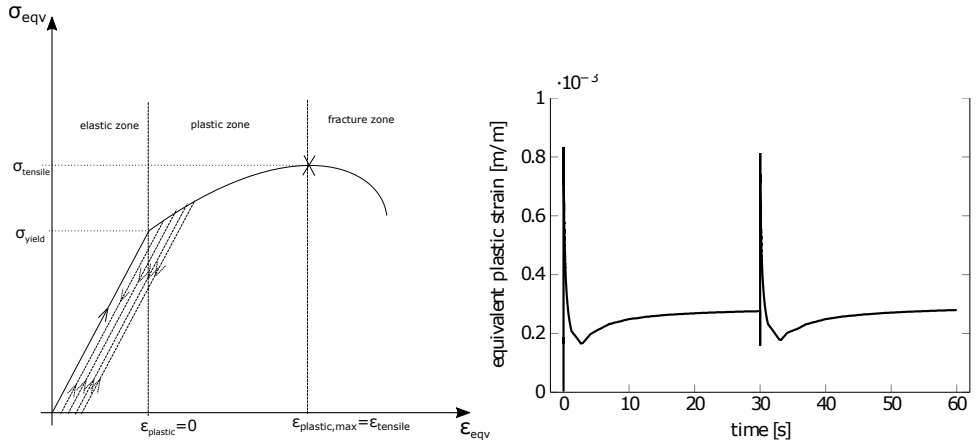

Figure 5. (a) Schematic engineering stress-strain curve showing heating and cooling phases in the plastic regime. (b) Equivalent plastic strain in the F16 stopper core under its current beam scenario.

5 Design of a new PS stopper core

This section is about a new stopper core designed to be structurally safe under upgraded beam scenarios and conform to beam-attenuation requirements. For standardization we aim for a common

2019 JINST 14 T01011

stopper and core design for all PS complex.

For design simplification the core has no active cooling system. In our analysis the core is passively cooled only through radiation to the vacuum chamber.

5.1 Beam parameters

The core takes several repeated beam pulses while moving from OUT-BEAM to IN-BEAM positions. The slowest core nowadays takes about 17 seconds between both positions. Knowing the smallest pulse repetition rate of all beam scenarios is 1.2 s a beam stopper is impacted by 15 repeated pulses. We use this number of repeated pulses as a design requirement. Although the beam could hit different spots on the core we assume in our analyses the repeated pulses hit only the core center.

The most damaging beam is the upgraded beam for the F16 line (2.3×10^{13} protons per pulse, 26 GeV/c, beam sizes $\sigma_x = 1.5$ mm and $\sigma_y = 1.39$ mm). Our beam parameters for validating the core integrity has the same intensity, energy and beam size as the most damaging beam with a repetition rate of 1.2 s following the shortest repetition rate in the PS complex [8].

5.2 Beam attenuation

In order to maintain the current beam-attenuation performance we keep the same accumulated multiples of the inelastic nuclear scattering length (λ_{inel}) in each beam line (table 4). The East Area is the most protected facility because of the high number of spills in a supercycle of the extracted beam. The nuclear interaction length is calculated for steel at different proton energies: $\lambda_{2.0\text{GeV}} = 14.97$ cm and $\lambda_{20-26\text{GeV/c}} = 15.56$ cm.

Table 4. Total protection length required in multiples of λ_{inel} for today's beam lines.

Beam line	proton energy [GeV]	total length [mm]	multiples of λ_{inel} required	number of $3.75\lambda_{\text{inel}}$ cores required
BTP	2.0	1100	7.3	2
BTY	2.0	600	3.9	1
EA-1.5m (both)	23.1	3000	19.0	5
EA-TX (each)	23.1	600	3.7	1
F16	25.1	1700	10.9	3
FTA	25.1	2200	14.2	4
FTN	19.1	2200	14.1	4

A core protection length of 3.75 λ_{inel} (table 4) is a fitting compromise between the EA, FTA and FTN lines while keeping the core length short. The other lines (BTP, BTY and F16) benefits from an increase in the total protection length.

Following the current electromagnetic containment of stainless steel stoppers with a radius of 100 mm we design our core with at least 5.7 R_m.

5.3 Single-block configuration

The new material must have a high yield strength in order to prevent permanent deformation. In addition high thermal-shock resistance (R_t, eq. 5.1) and low temperature rise per beam pulse reduce

2019 JINST 14 T01011

thermal stress peaks. Stainless steel (SS304L) is again proven to be unsuitable compared to other materials (table 5).

$$R_t = \frac{k\sigma_y(1-\nu^2)}{\alpha E} \tag{5.1}$$

Here α is the coefficient of thermal expansion.

Table 5. Material comparison for a new beam stopper core. Temperature-dependant properties from [37]. In this table properties are evaluated at room temperature. Peak temperature rise per beam pulse ΔT_{peak} considers a single proton beam impact at 2.3×10^{13} ppp and 26 GeV/c.

Material	σ_y [MPa]	R_t [W/m]	ΔT_{peak} [°C]	repeated pulses for $\sigma_e/\sigma_y(T) > 1$	λ_{inel} at 26 GeV/c [cm]
Antico 100	240	20 500	80	indefinite	37.5
TiAl6V4	938	6 020	130	132	26.8
SS304L	168	675	228	1	15.6
Inconel 718	1030	4 200	230	7	15.5
CuCr1Zr	290	47 000	240	1	14.7
TZM	812	114 000	420	1	14.5
Inermet180	517	27 060	651	1	9.82

Low-density materials such as aluminum (Antico 100) and titanium (TiAl6V4) alloys have low peak temperature rise and can withstand several repeated pulses. Nevertheless stopper cores with those materials have to be very long for personnel protection due to their long nuclear interaction lengths.

The copper alloy CuCr1Zr fails the safety criterion on one single pulse impact despite its high thermal-shock resistance. The nickel alloy Inconel 718 is the only high-density materials able to withstand repeated pulses thanks to its high yield strength. Although the shock resistance of the molybdenum alloy TZM is the highest the peak temperature rise per pulse in this material is also high, making it less suitable as a core material than Inconel 718.

5.4 Diluter-absorber configuration

This configuration consists of a diluter out of a low-density material that absorbs part of the incoming beam energy leaving a smaller amount of energy to a downstream absorber out of a high-density material (figure 6). Introducing a 300-mm long titanium cylinder reduces the peak temperature rise in our reference Inconel 718 absorber by 52%.

A titanium-alloy diluter absorbs more beam energy for the same material length than an aluminum alloy. In addition the beam attenuation in the titanium alloy is stronger allowing the diluter to be more compact for the same beam attenuation.

The amount of repeated pulses a CuCr1Zr absorber withstands increases to 86 by elongating the titanium diluter to 300 mm. This amount is increased to only 51 in an Inconel 718 absorber.

Using this configuration we select a 250-mm long titanium diluter (figure 7a) followed by a 415-mm long absorber made of CuCr1Zr, profiting from the high thermal conductivity, thermal-shock resistance and affordability of this material. This core provides a total of 3.75 λ_{inel} (diluter: 0.95 λ_{inel}; absorber: 2.8 λ_{inel}) withstanding 20 repeated pulses of the required beam (figure 7b).

2019 JINST 14 T01011

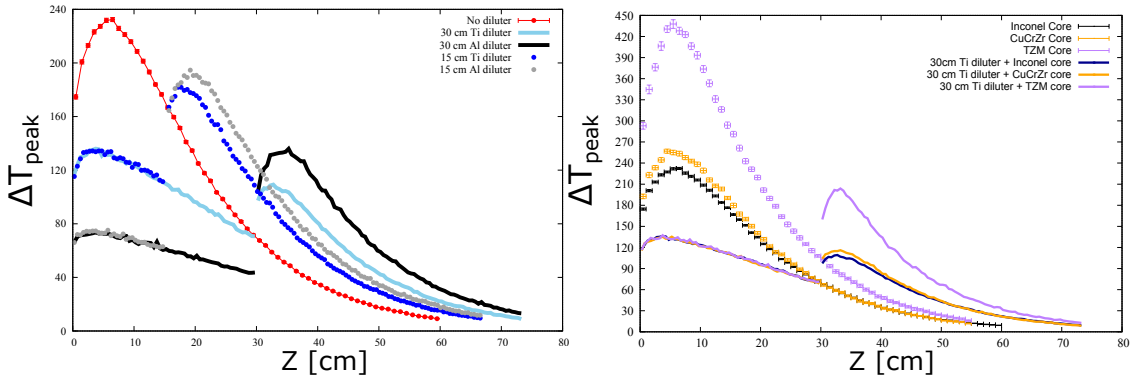

(a) **(b)**

Figure 6. (a) Sensitivity analysis on the diluter material. Different lengths of an aluminum-alloy and a titanium-alloy diluter in front of a Inconel 718 absorber are analyzed. (b) Sensitivity analysis on the absorber material. A 300-mm long titanium-alloy diluter is chosen as the baseline for this analysis.

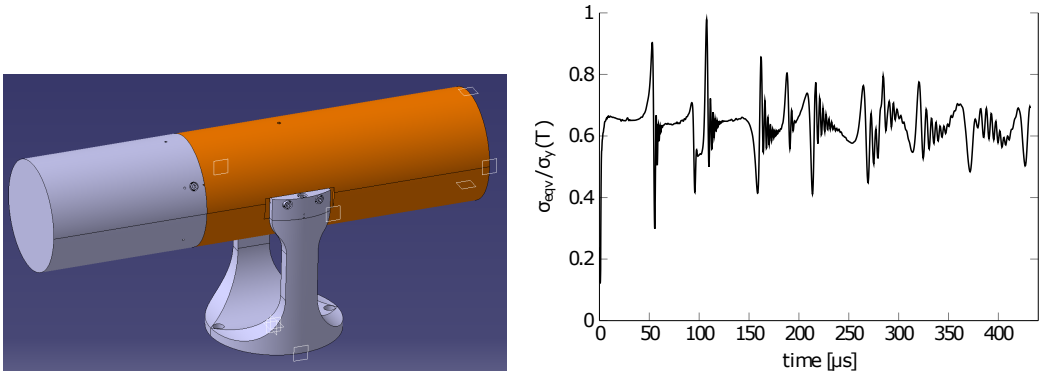

(a) **(b)**

Figure 7. (a) Diluter-absorber core configuration with an diluter out of TiAl6V4 (in grey) as and an absorber out of CuCr1Zr (in orange). (b) Ratio between the equivalent stresses and the temperature-dependent yield strength at the point of maximum $\sigma_{\text{eqv}}/\sigma_{\text{y}}$ right after 20 repeated pulses in the CuCr1Zr absorber.

The maximum temperature after 20 repeated pulses in the diluter is $T_{\text{max}} = 380.0^{\text{o}}$C. In the absorber $T_{\text{max}} = 223.7^{\text{o}}$C, max $\sigma_{\text{eqv}}/\sigma_{\text{y}}(T) = 0.98$ and max $\sigma_{\text{eqv}} = 257.6$ MPa.

After 15 repeated pulses the beam stopper has to be left to passively cool down in order to avoid the increase of thermal strains. Considering an optical emissivity of titanium $\epsilon = 0.19$ and copper $\epsilon = 0.07$, a homogeneous temperature around 28.6°C in the whole diluter is reached after 87 minutes, whereas a homogeneous temperature around 34.0°C is achieved in 29 minutes in the absorber.

5.5 High-density sliced diluter

In order to reduce the core length while keeping the same attenuation factor of 3.75 λ_{inel} we introduce a high-density sliced diluter. Under energy deposition from beam impacts the thin slices allow the material to freely expand in the beam axis, reducing the axial stress component.

2019 JINST 14 T01011

Figure 8 shows a massive Inconel 718 cylinder hit by beam presents permanent deformation while a sliced configuration prevents the material from plastic deformation. In a full-block core out of Inconel 718 max $\sigma_{eqv}/\sigma_y(T) = 1.34$ using a fully elastic material model, max $\sigma_{eqv} = 1120$ MPa and $T_{max} = 707^o$C. In a core with 20-mm thick slices out of Inconel 718, max $\sigma_{eqv}/\sigma_y(T) = 0.88$, max $\sigma_{eqv} = 776$ MPa and $T_{max} = 709^o$C. A sensitivity analysis for Inconel 718 and TZM slices (figure 8c) indicates each material has an optimum slice thickness for low equivalent stresses.

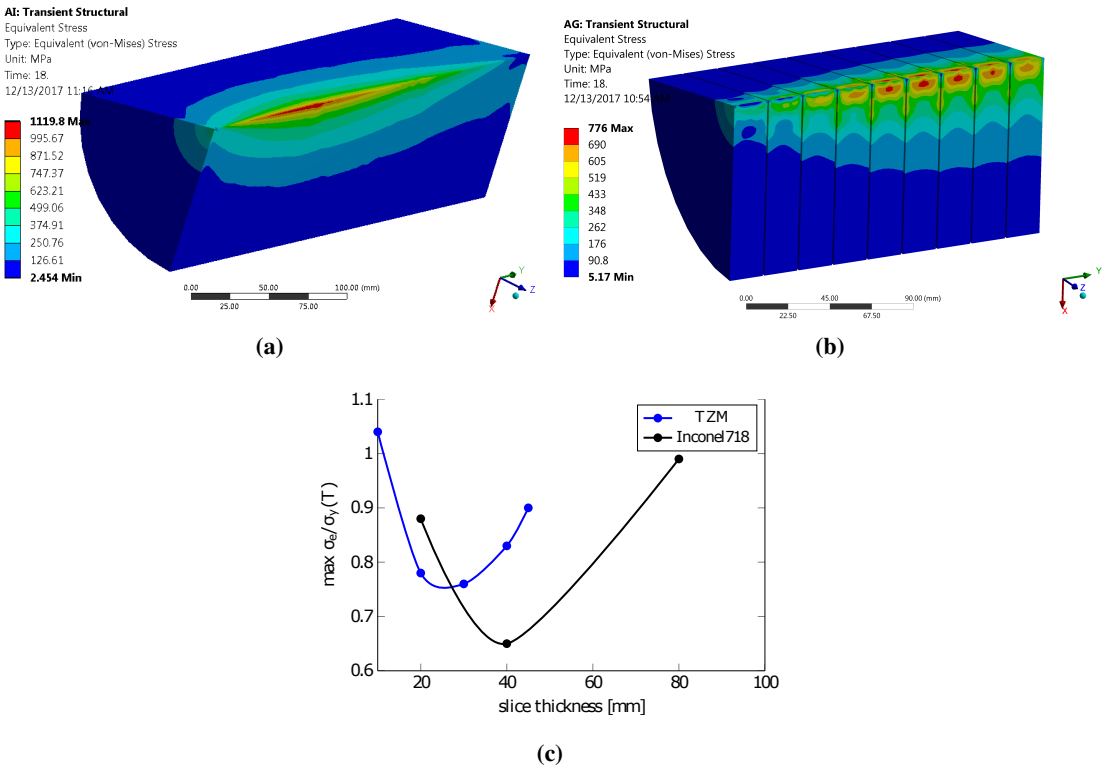

Figure 8. Maximum pulsed equivalent stress over 15 repeated pulses. (a) Full-block core out of Inconel 718. (b) Sliced core with 20-mm thick slices out of Inconel 718. (c) Max $\sigma_{eqv}/\sigma_y(T)$ for various thicknesses of a sliced diluter out of TZM and Inconel 718 after 15 repeated pulses.

Based on the previous titanium-copper core configuration our new diluter must have a minimum attenuation factor of 0.94 λ_{inel} for thermo-mechanical integrity of the CuCr1Zr absorber. Taking a slice thickness of Inconel 718 at 40 mm we introduce a compact stopper core with four Inconel 718 slices followed by a CuCr1Zr massive absorber. The total length of this core is 564 mm (figure 9) with gaps between parts of 1 mm for allowing thermal expansion of the slices in beam direction. All four slices of Inconel 718 together provide a diluter attenuation factor of 1.03 λ_{inel}. Keeping the diameter of the stopper core at 200 mm the sliced Inconel 718 diluter has 6.7 Rm ($R_m = 14.9$ mm [28]) while the CuCr1Zr absorber block has 6.4 R_m ($R_m = 15.6$ mm [28]).

Figure 10 presents the thermal and equivalent-stress distribution in terms of $\sigma_{eqv}/\sigma_y(T)$ in the new sliced core right after 15 repeated pulses. The maximum equivalent stress is 601 MPa in the Inconel slices and 218 MPa in the CuCr1Zr absorber. After repeated pulses the core must be left to cool down for 16 minutes for its maximum temperature to reduce to 40°C.

2019 JINST 14 T01011

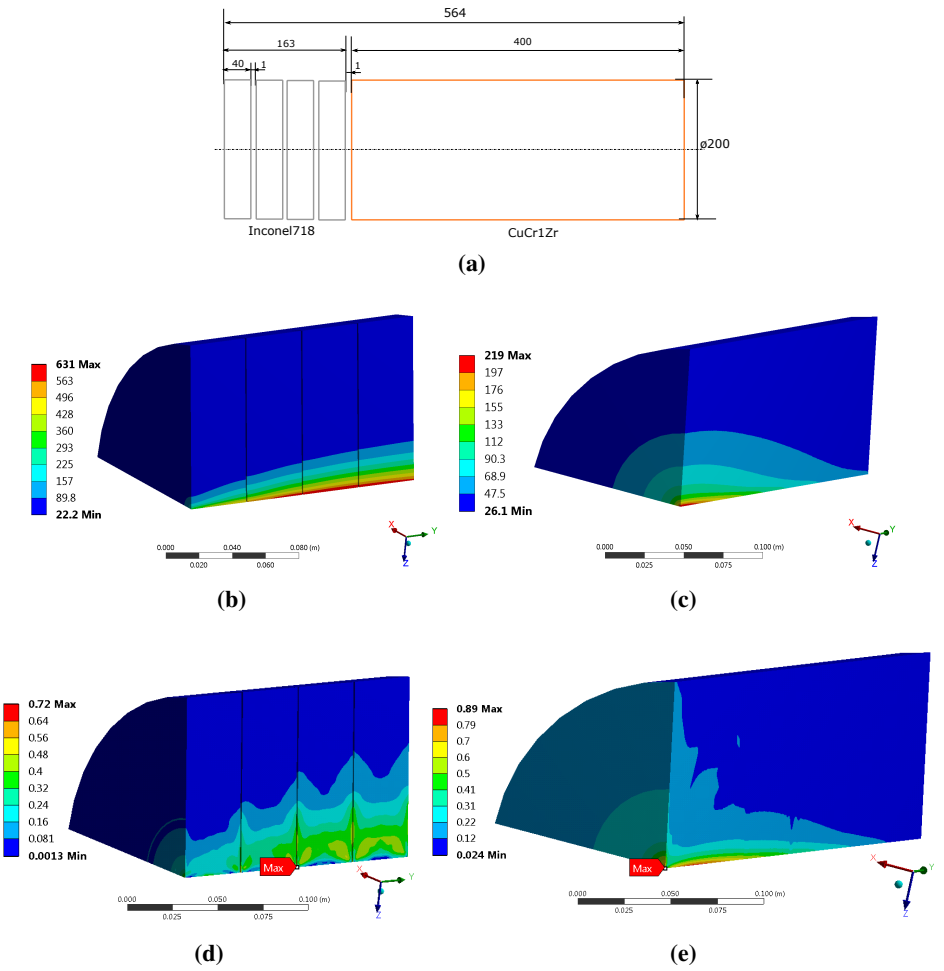

Figure 9. (a) Schematic representation of the new PS-complex stopper core. Temperature distribution and maximum ratio $\sigma_{\mathrm{eqv}}/\sigma_{\mathrm{y}}(T)$ in the sliced Inconel 718 diluter (b,d) and in the CuCr1Zr absorber (c,e) right after 15 repeated pulses.

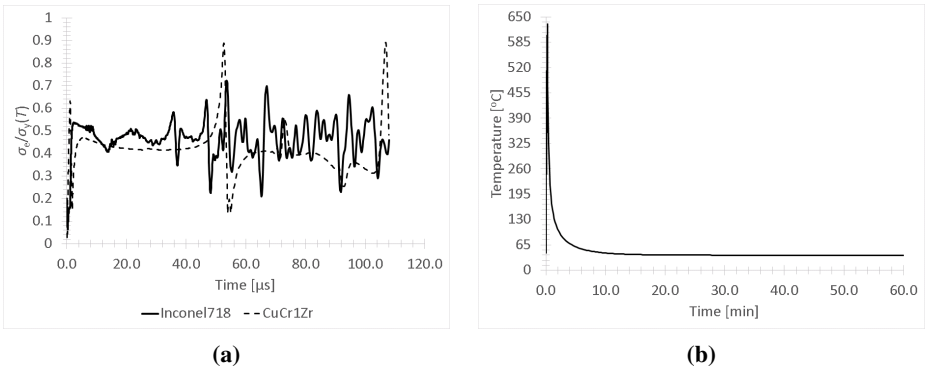

Figure 10. (a) Ratio $\sigma_{\mathrm{eqv}}/\sigma_{\mathrm{y}}(T)$ evaluated at the point where this ratio is the highest right after 15 repeated pulses. (b) Maximum temperature in the core after 15 repeated pulses.

2019 JINST 14 T01011

5.6 Radiation protection aspects

At an intensity of 23×10^{12} protons per pulse and high energies the new core emits a similar neutron spectrum as the previous steel core (figure 11a).

After the impact of 15 consecutive pulses separated by 1.2 seconds with an intensity of 23×10^{12} protons per pulse, the maximum ambient dose equivalent rate reached at 40 cm from the stopper surface is 3.5 mSv/h after 1 hour of cool-down time and 0.2 mSv/h after 1 day of cool-down time (figure 11b). These ambient dose rates are lower than the ones usually found at the extraction equipment located upstream in the PS machine [38].

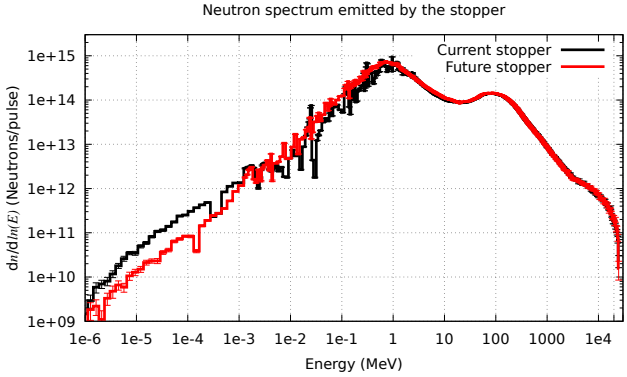

(a)

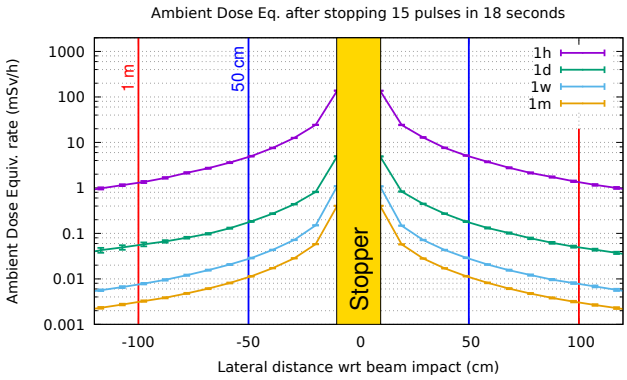

(b)

Figure 11. (a) Neutron spectra emerging from the current and future beam stopper after the impact of a 26 GeV/c beam of 23×10^{12} protons. (b) Residual ambient dose equivalent rates after the impact of 15 repeated pulses in the new core for different cool-down times.

The required cool-down times depend on the activity to be performed, being defined together with the CERN Radiation Protection group [38]. All accesses to the beam stoppers, including those for inspection, maintenance or repair, are accompanied by the CERN Radiation Protection group to ensure proper radiation protection of these activities.

2019 JINST 14 T01011

6 Conceptual design of the new beam stopper

Instead of the long 2c-type design we opt for a beam stopper out of a single core in a vacuum chamber for easier maintainability and mechanical integration in the beam line. Figure 12 presents a conceptual beam stopper design for the PS complex [39].

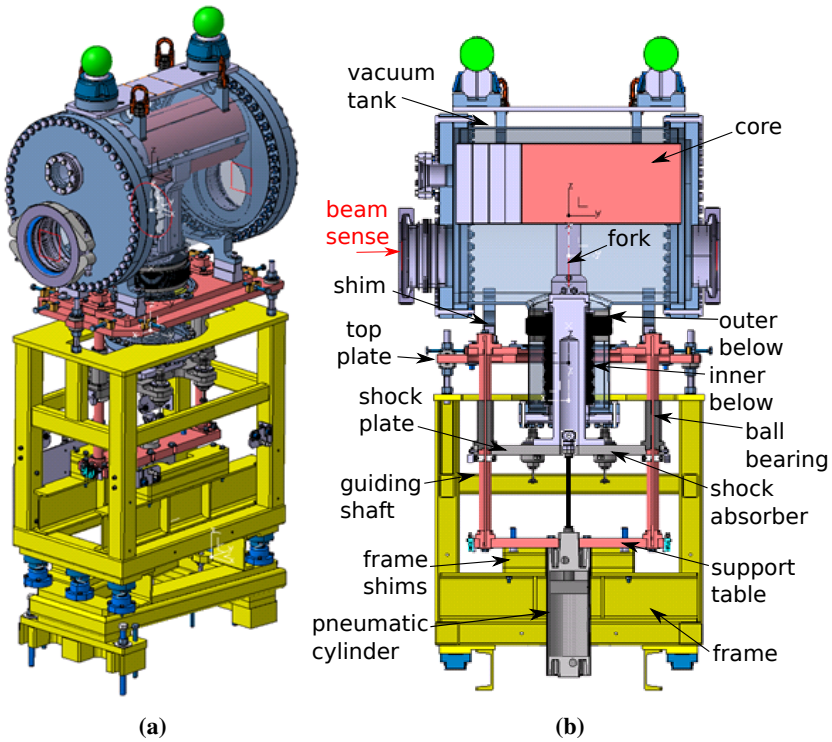

Figure 12. (a) Schematic drawing of the new beam stopper [39]. (b) Cut view [39].

In the new beam stopper the core is held over the beam line by a fork linked to a pneumatic cylinder and connected to a shock plate having shock absorbers and ball bearings. The tank is supported by the top table and the outer bellow. The top table orients the tank in the horizontal plane. The outer bellow allows the core and tank axes to be aligned with the beam line. This vertical alignment is set up by means of shims placed under the tank allowing a maximum tilt of 4°. In the BTY line the new beam stopper must be moved from the current position with 11° to a position with a maximum tilt of 6.3° in order to still meet the electromagnetic containment requirement in the core (5.7 R_m).

During beam operation the core stays in OUT-BEAM position supported by an inner bellow (figure 13). Whenever members of the personnel wants or forces the access in a downstream area or in fail-safe cases, the pneumatic cylinder is de-pressurized and the core moves to IN-BEAM position. The shock plate slides in the guiding shafts connected to the top table. The fall of the core is damped through shock absorbers on the frame shims.

A dedicated test bench using a pneumatically controlled mechanism demonstrated the core travels from OUT-BEAM to IN-BEAM position in less than 2.0 s [39, 40] using a double actuating cylinder. This demonstrator used massive iron blocks equivalent to the total forces the core assembly exerts on the pneumatic actuator and the shock absorbers during the its fall.

2019 JINST 14 T01011

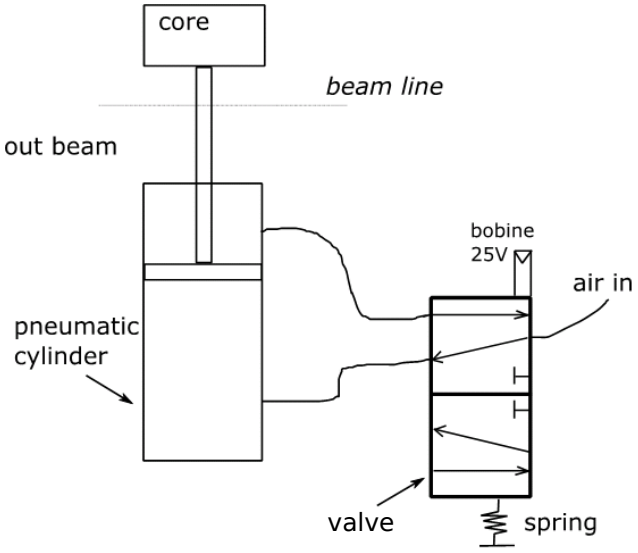

Figure 13. Schematic representation of the double pneumatic actuation of the new core in OUT-BEAM position.

7 Conclusions

We described the performance of the current beam stoppers for personnel safety in the PS complex at CERN. Their steel cores reaches the elastic material limit under a single beam pulse impact with 5.8×10^{12} particles at 26 GeV/c.

We introduced guidelines for the design of a new core in terms of multiples of the nuclear interaction length (λ_{inel}) and the electromagnetic containment in Moliere radii (R_{m}). The new core is designed for 15 repeated beam impacts with 23×10^{12} protons per pulse at 26 GeV/c and beam sizes $\sigma_{\text{x}} = 1.5$ mm and $\sigma_{\text{y}} = 1.39$ mm based on the most damaging beam upgrade scenarios.

A comparison of materials with regards to the thermal-shock resistance and peak temperature rise in beam-intercepting metals showed no high-density material directly withstands 15 repeated beam pulses. We proposed a diluter-absorber configuration in which a low-density diluter out of the titanium alloy Ti6Al4V dampens the peak temperature rise in a high-density absorber out of the copper alloy CuCr1Zr.

For even shorter stopper cores for personnel safety this paper brought out high-density sliced diluters. This diluter allows the material to freely expand in beam axis during repeated beam impacts reducing thermal stresses. The new core is 564-mm long, has a diameter of 200 mm and consists of a sliced diluter out of the nickel-alloy Inconel 718 and a massive absorber out of the copper-alloy CuCr1Zr. It provides 3.75 λ_{inel} of nuclear interaction length and at least 6.4 R_{m} of electromagnetic containment.

In the conceptual design of the new beam stopper the core is held by a bellowed fork in vacuum linked to a pneumatic actuator, vertically descending in beam line in less than 2.0 s. The new beam stopper and its compact sliced-diluter core replace five previous designs in the PS complex and will be replicated in each beam line according to beam-attenuation requirements. First prototypes of the conceptual design of the beam stopper will be tested in the beginning of 2019.

2019 JINST 14 T01011

Acknowledgments

The authors want to thank: Robert Froeschl for his assistance and guidance in radiation protection issues; Pablo Ortega Garcia for first FLUKA simulations; Dylan Baillard for his work and engagement in the construction of the pneumatic demonstrator; Riccardo Peron, Marc Timmins, Mathis Dole for their work on the design of the new beam stopper; Ramon Folch for project kick-off; the LIU-PSB, LIU-PS, PS-consolidation and EA-renovation teams on their support in accelerator and beam-related parameters; and Alexandre Pilan Zanoni for proofreading.

References

[1] n_TOF collaboration, *Status and outlook of the neutron time-of-flight facility n_TOF at CERN*, *Nucl. Instrum. Meth.* **B 261** (2007) 925.

[2] M. Hori and J. Walz, *Physics at CERN's Antiproton Decelerator*, *Prog. Part. Nucl. Phys.* **72** (2013) 206 [arXiv:1304.3721].

[3] F. Ravotti, E. Matli, B. Gkotse, M. Moll, P. Lima and M. Glaser, *A new high-intensity proton irradiation facility at the CERN PS East Area*, PoS(TIPP2014)354.

[4] D. Chapuis, F. Chapuis, G. Dumont, J.L. Duran-Lopez, L. Hammouti, S. Hutchins et al., *Specification des elements d'acces et inter-verrouillage de la zone booster*, PSB-Y-ES-0001, CERN, 2015.

[5] D. Chapuis, F. Chapuis, G. Dumont, J.L. Duran-Lopez, L. Hammouti, S. Hutchins et al., *Specification des elements d'acces et inter-verrouillage de la zone switch-yard*, EDMS 990206, CERN, 2015.

[6] A. Funken, *Definition et inventaire des EIS-Faisceau et EIS-Machine*, ATS-S-ER-0001, CERN, 2015.

[7] M. Harris, H. Kropf and S. Turner, *Desgin and control of the beam stoppers and dumps for the ISR beam transfer system*, CERN-ISR-OP-EN/71-60, CERN, 1971.

[8] R. Steerenberg, *PS beam spot sizes for the design of new beam stoppers (TT2 - FTN - FTA)*, EDMS 1612294, CERN, 2016.

[9] L. Rossi, *LHC upgrade plans: options and strategy*, in *Proceedings of the 2nd International Particle Accelerator Conference*, San Sebastian, Spain, 4–9 September 2011, pp. 908–912 [TUYA02].

[10] R. Garoby, H. Damerau, S. Gilardoni, B. Goddard, K. Hanke, A. Lombardi et al., *Status and Plans for the Upgrade of the LHC injectors*, in *Proceedings of the 4th International Particle Accelerator Conference*, Shanghai, China, 13–17 May 2013, pp. 3936–3938 [THPWO077].

[11] C. Maglioni and R. Folch, *Definition of Beam Stoppers, Beam Dumps and Stopper/Dumps*, EDMS 1283556, CERN, 2015.

[12] J. Lendaro and M. Butcher, *Beam stoppers in the PS complex - Electronics & Control System*, EDMS 1278742, CERN, 2013.

[13] A. Ferrari, P.R. Sala, A. Fasso and J. Ranft, *FLUKA: A multi-particle transport code (program version 2005)*, SLAC-R-773, Stanford Linear Accelerator Center, Stanford University, Stanford, CA 94309, 2005.

[14] T. Böhlen, F. Cerutti, M. Chin, A. Fassò, A. Ferrari, P. Ortega et al., *The FLUKA code: developments and challenges for high energy and medical applications*, *Nucl. Data Sheets* **120** (2014) 211.

[15] *ANSYS Academic Research, Release 17.1 (manual)*.

[16] N.M. Newmark, *A method of computation for structural dynamics*, *J. Eng. Mech. ASCE* **85** (1959) 67.

2019 JINST 14 T01011

[17] H. Hilber, T. Hughes and R. Talor, *Improved numerical dissipation for time integration algorithms in structural dynamics*, *Earthq. Eng. Struct. D.* **5** (1977) 282.

[18] R. Courant, K. Friedrichs and H. Lewy, *On the partial difference equations of mathematical physics*, *IBM J. Res. Dev.* **11** (1967) 215.

[19] A. Pilan Zanoni, *Method for thermal and structural evaluation of shallow intense-beam deposition in matter*, *Phys. Rev. Accel. Beams* **21** (2018) 054801.

[20] M. Ishihara, J. Sumita, T. Shibata, T. Iyoku and T. Oku, *Principle design and data of graphite components*, *Nucl. Eng. Des.* **233** (2004) 251.

[21] R. von Mises, *Mechanik der festen Körper im plastisch-deformablen Zustand*, *Nachrichten von der Gesellschaft der Wissenschaften zu Göttingen, Mathematisch-Physikalische Klasse* **1913** (1913) 582.

[22] R.M. Christensen, *The theory of materials failure*, Oxford University Press (2013).

[23] A. Brown and H. Suit, *The centenary of the discovery of the bragg peak*, *Radiother. Oncol.* **73** (2004) 265.

[24] R.H. Dicke and J. Marshall Jr, *Inelastic scattering of protons*, *Phys. Rev.* **63** (1943) 86.

[25] B.R. Martin and G. Shaw, *Particle physics*, John Wiley & Sons (2017).

[26] G. Bathow, E. Freytag, M. Koebberling, K. Tesch and R. Kajikawa, *Measurements of the longitudinal and lateral development of electromagnetic cascades in lead, copper and aluminum at 6 GeV*, *Nucl. Phys.* **B 20** (1970) 592.

[27] Particle Data Group collaboration, *Review of Particle Physics*, *Chin. Phys.* **C 40** (2016) 100001.

[28] *PDG - Particle Data Group, atomic and nuclear properties of materials for more than 300 materials*, 2016.

[29] C. Bracco and G.P. Di Giovanni, *Beam Parameters for the Validation of the Beam Stoppers in the PSB Injection Line in the Framework of the LIU-PSB Upgrade*, PSB-TSSTP-ES-0001, CERN, 2016.

[30] J. Abelleira, *Beam parameters for the validation of the beam stopper in the PSB-PS line (BTP) within the LIU-PSB upgrade*, PSB-TSSTP-ES-0002, CERN, 2016.

[31] V. Forte, M.A. Fraser and G.P. Di Giovanni, *Beam Parameters for the Validation of the Beam Stopper in the PSB - ISOLDE line (BTY) for the Present and Upgraded Operational Scenarios*, PSB-TBS-EP-0001, CERN, 2018.

[32] M. Lazzaroni, J. Bernhard and E. Harrouch, *Beam Stopper, Stopper Dump and Target. Context: East-Area Renovation Project*, EDMS 1786687, CERN, 2018.

[33] F. Leaux and S. Sgobba, *Stainless steel round bars for Vacuum Applications*, EDMS 790544, CERN, 2016.

[34] A. Funken, *Minutes of the 2nd meeting related to EIS-Beam for the PS Booster with Linac4 and Linac3 beams*, LIU-PM-MIN-0295 v.1, CERN 2016.

[35] C. Maglioni, F. Loprete and S. Cimmino, *Beam stopper L4T*, L4-T-ES-0008, CERN, 2015.

[36] J.F. Dempsey, B.R. Antoun, V.J. Romero, G.W. Wellman, W.M. Scherzinger and S. Grange, *Temperature dependent ductile material failure constitutive modeling with validation experiments*, in *Challenges in Mechanics of Time-Dependent Materials and Processes in Conventional and Multifunctional Materials, Volume 2*, Springer (2013), pp. 7–15.

[37] EN-STI-TCD material database, CERN, 2018.

2019 JINST 14 T01011

[38] R. Froeschl and F. Pozzi, *Radiation Protection Feedback on the PS Beam Stoppers Upgrade*, EDMS 2009197, CERN-HSE-RP-AS, 2018.

[39] A. Pilan Zanoni, E. Grenier-Boley, R. Peron, M. Dole and M. Timmins, *Engineering and Design of the new PS Beam Stoppers*, EDMS 1979131, CERN, 2018, in work.

[40] D. Baillard and E. Grenier-Boley, *Internship beam stopper LS2 presentation*, EDMS 1865799, CERN, 2017, in work.

2019 JINST 14 T01011